Article

Operation and Control of a PV-Wind Hybrid System under Various Weather and Loading Conditions

Mostafa S. Fathy [1], Hilmy Awad [2,*], Hosam Hegarzy [2] and Elwy E. Elkholy [3]

[1] College of Technology Ministry of Higher Education Cairo, Egypt; mostafa.sayed77@yahoo.com
[2] Faculty of Industrial Education Helwan Univ, Cairo- Egypt; hossamyh@hotmail.com
[3] Engineering Dept., Faculty of Engineering Menoufia Univ, Egypt
* Correspondence: hilmy_awad@yahoo.com; Tel.: +201023106300

Abstract: In this paper, an extensive study on the operation, control and performance of a hybrid photovoltaic and wind turbine (PV-WT) system is presented. The study includes the operation of the hybrid systems under different weather conditions which are reflected on a change in the wind speed and irradiance. Various loading conditions are investigated such a change in active and reactive power demands for static and dynamic loads. The performance of the hybrid system is examined via MATLAB/SIMULINK simulations.

Keywords: photovoltaic (PV); maximum power point tracking (MPPT); doubly-fed induction generator (DFIG)

1. Introduction

Since the National Electrical Network of Egypt relies mainly on the thermal power stations that require a considerable amount of fossil fuels and pollute the environment, the Supreme Council of Energy has planned for the renewable energy sources to generate about 20 % of the national demand by 2020 [1]. It is clear that the weather of Egypt and its geographic location make it a potential candidate to lead the region in the field of renewable energy and possibly exports electric power to the neighbours. Th idea is to focus more on harnessing of the renewable energy sources in order to gradually replace the conventional electrical grid aiming at minimizing the electric power cost and serve the environment.

The photovoltaic energy is one of the promising technologies and forms a pillar of the so called green energy sources. However, the capital and installation costs of solar power stations are still rather high. Consequently, an improvement of the efficiency of solar systems is offsets some of the cost. Many methods and techniques have been proposed in literature in order to maximize the efficiency such as maximum power point tracking (MPPT) [2]. A typical PV system is depicted in Fig.1a where it may include a battery in the case of standalone applications.

The main issue with most of the renewable energy sources is there intermittent nature which dictates the necessity of merging more than one source in order to ensure the continuity of the power supply to the loads. Many combinations have been studied and one those is considered in this work which is an integration of photovoltaic and wind power systems.

The doubly-fed induction generator (DFIG) is widely used in wind power applications due the high flexibility in control and its rigid structure. Flexibility in this context implies that the rotor circuit can take or give electric power to the system depending on the rotational speed. Also, it can operate at the synchronous speed at which neither takes or gives power [3]. More importantly, the active and reactive powers can be controlled independently. A DFIG-based wind power system is shown in Fig.1b where two converters are needed: grid-side converter (GSC) and rotor-side converter (RSC). In some design cases, a gear box (GB) is required.

From Fig. 1 a and b, it is noted that in the case of a hybrid PV-Wind system, the two sources can be joined at the inverter output terminals after the filter as depicted in Fig. 2. Such layout has been proposed in [4]. The PV inverter can be eliminated in order to simplify the circuit and perhaps the

Preprints (www.preprints.org) | NOT PEER-REVIEWED | Posted: 26 November 2017 doi:10.20944/preprints201711.0169.v1

cost can be reduced. In this scenario, the link between the PV and Wind turbine is at the DC output terminals of the MPPT and the middle points between the two wind concreters [5] as displayed in Fig. 3.

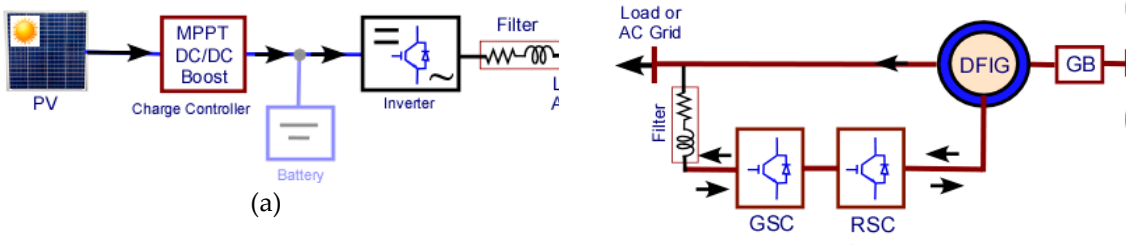

(a) (b)

Fig.1. (**a**) Typical PV system; (**b**) Typical wind turbine system.

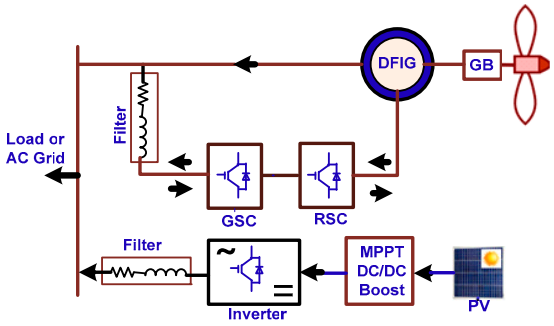

(a)

Fig. 2 Linking the PV and Wind Turbine at the AC outputs after the filter.

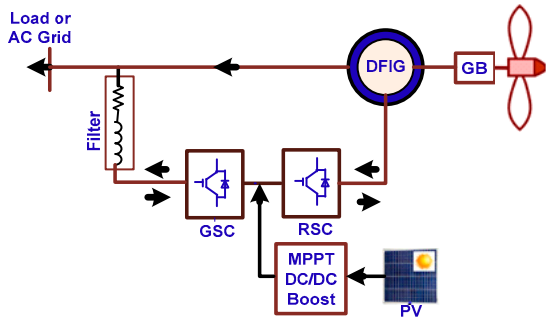

(b)

Fig. 3 Linking the PV and Wind Turbine at the DC terminals.

Modeling and simulation of a hybrid PV and DFIG-based wind system was found in literature such as [6]. A storage system composed of super capacitor and a battery has been added to the hybrid system and a comprehensive dynamic analysis for grid applications is investigated in [7]. Adding the storage system helps in maintaining the power to the loads/grid, particularly in the case of grid disturbances. Another work on hybrid PV-Wind system is presented in [8]. In this work, the average monthly meteorological data for the city of Basrah, Iraq are taken as the input parameters, which make the presented models applicable.

In this paper, an extensive study on the operation and performance of a hybrid PV-Wind system is presented. A description of the system under investigation is given in Section II. Section III shows the applied controllers in order to fulfil the load requirements. The simulation results using MATLAB/Simulink are displayed in Section IV. Section V states the study conclusions.

Preprints (www.preprints.org) | NOT PEER-REVIEWED | Posted: 26 November 2017 doi:10.20944/preprints201711.0169.v1

2. SYSTEM DESCRIPTION

The hybrid system consists of a PV and wind turbine power systems with their components as described in Section I. The models of both systems are well-described in literature and are briefly explained here for the purpose of reader's comfort.

A. Modeling of photovoltaic:

The solar cell/module is modelled by an equivalent circuit like the one shown in Fig.4. A dc current source (I_{ph}) is connected in parallel with a reverse-biased diode and a shunt resistance. The shunt resistance (R_{sh}) models a macroscopic defect in the solar cell resulting in an alternative path for the photocurrent. A series resistance (R_s) is included in order to model the power loss through the joints and wire connections inside the cell [9].

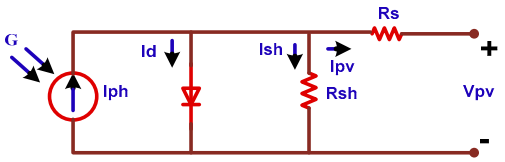

Fig. 4 The equivalent circuit of photovoltaic.

The mathematical of PV model is given by the equation below.

$$I_{pv} = N_p.I_{ph} - N_p.I_d - I_{sh} \quad (1)$$

$$I_{ph} = [I_{sh} + K_i(T_c - T_{ref})]\left(\frac{G}{1000}\right) \quad (2)$$

Where G is the amount of irradiance and I_{pv} is the PV current. I_{ph} is the photocurrent and I_d is the current through the diode. I_s represents the diode saturation current and q is the electron charge. T_c is the operating temperature, and T_{ref} is the reference temperature.

B. Modeling of wind turbine doubly-fed induction generator

The output power of the wind turbine is given by equation (3), where C_p is the power coefficient, ρ is air density, A is swept area of rotor blades, V is the wind velocity, λ is the tip speed ratio (TSR) and β is the pitch angle. C_p characterizes the efficiency of the conversion process from a wind power to a mechanical rotational power. The C_p is an indication of the maximum power that can converted to mechanical power at a specified wind speed. It is a function of the tip-speed ratio and the blade pitch angle. The blade pitch angle can be controlled by using a "pitch-controller" and the tip-speed ratio [10].

$$P_m = 0.5\,\rho\,A V^3\,C_p(\lambda,\beta) \quad (3)$$

3. APPLIED CONTROLLERS

The PV system is controlled by the MPPT at which the perturb and observe method is adapted. If the reader is interested in this topic, he/she can refer to literature such as [11]

The Grid-Side Converter Controller

The control of the GSC aims to regulate the voltage of the DC link that is between the back-to-back converters, irrespective of the rotor power fluctuations. Sine the vector control is adapted, the active and reactive powers can be controlled indecently between the GSC and the grid. The GSC controller consists of two control loops: an inner loop to regulate the reactive power flow and an outer loop to control the DC voltage. The outputs of the outer control loop are the reference values of the direct- and quadrature- axis current components as given by equations (4) and (5). In other words, the magnitude and the phase angle of the output current of the GSC are obtained by the outer control loop [12]. In (5), $V_{L\text{-}ref}$ and V_L are the reference and the actual values of the load/grid voltage, respectively.

Preprints (www.preprints.org) | NOT PEER-REVIEWED | Posted: 26 November 2017 doi:10.20944/preprints201711.0169.v1

$$I_{\mathrm{d}}^{*} = K_{\mathrm{p1}}(V_{\mathrm{dc}}^{*} - V_{\mathrm{dc}}) + K_{\mathrm{i1}}\int (V_{\mathrm{dc}}^{*} - V_{\mathrm{dc}})dt \qquad (4)$$

$$I_{\mathrm{q}}^{*} = K_{\mathrm{p2}}(V_{\mathrm{L\text{-}ref}} - V_{\mathrm{L}}) + K_{\mathrm{i2}}\int (V_{\mathrm{L\text{-}ref}} - V_{\mathrm{L}})dt \qquad (5)$$

After calculating the current components, they are used to determine the magnitude and phase angle of the output GSC voltage through the calculations of the direct- and quadrature axis components V_{d}^{*} and V_{q}^{*} as given by equations (6) and (7).

$$V_{\mathrm{d}}^{*} = K_{\mathrm{p3}}(I_{\mathrm{d}}^{*} - I_{\mathrm{d}}) + K_{\mathrm{i3}}\int (I_{\mathrm{d}}^{*} - I_{\mathrm{d}})dt - \omega L_{\mathrm{f}} I_{\mathrm{q}} + V_{\mathrm{sd}} \qquad (6)$$

$$V_{\mathrm{q}}^{*} = K_{\mathrm{p3}}(I_{\mathrm{q}}^{*} - I_{\mathrm{q}}) + K_{\mathrm{i3}}\int (I_{\mathrm{q}}^{*} - I_{\mathrm{q}})dt + \omega L_{\mathrm{f}} I_{\mathrm{d}} + V_{\mathrm{sq}} \qquad (7)$$

A schematic diagram of the GSC controllers is depicted in Fig. 5.

The Rotor Side Converter Controller

The RSC mainly controls the power absorbed or supplied by the rotor of the DFIG via providing the proper amounts of the rotor current magnitude and phase angle. This implies that the RSC determines the rotor flux position and magnitude with respect to stator flux position and consequently the required torque is applied on the rotor shaft. The RSC uses a torque controller to regulate the wind turbine output power and the voltage (or reactive power) measured at the machine stator terminals [13]. The direct-axis component of the rotor current regulates the reactive power flow while the quadrature-axis component determines the shaft speed as given by equations (8) and (9).

$$I_{\mathrm{rd}}^{*} = K_{\mathrm{p}}(Q_{\mathrm{s}}^{*} - Q_{\mathrm{s}}) + K_{\mathrm{i}}\int (Q_{\mathrm{s}}^{*} - Q_{\mathrm{s}})dt \qquad (8)$$

$$I_{\mathrm{rq}}^{*} = K_{\mathrm{p}}(\omega_{\mathrm{r}}^{*} - \omega_{\mathrm{r}}) + K_{\mathrm{i}}\int (\omega_{\mathrm{r}}^{*} - \omega_{\mathrm{r}})dt \qquad (9)$$

$$V_{\mathrm{rd}}^{*} = K_{\mathrm{p4}}(I_{\mathrm{rd}}^{*} - I_{\mathrm{rd}}) + K_{\mathrm{i4}}\int (I_{\mathrm{rd}}^{*} - I_{\mathrm{rd}})dt - \omega_{\mathrm{slip}}\sigma L_{\mathrm{r}} I_{\mathrm{rq}} \qquad (10)$$

$$V_{\mathrm{rq}}^{*} = K_{\mathrm{p4}}(I_{\mathrm{rq}}^{*} - I_{\mathrm{rq}}) + K_{\mathrm{i4}}\int (I_{\mathrm{rq}}^{*} - I_{\mathrm{rq}})dt - \omega_{\mathrm{slip}}\left(L_{\mathrm{o}} i_{\mathrm{ms}} + \sigma L_{\mathrm{r}} I_{\mathrm{rq}}\right) \qquad (11)$$

The output voltage of the RSC is controlled by the direct- and quadrature-axis of RSC current as given by equations (10) and (11). A schematic diagram of the RSC controllers is depicted in Fig. 6. Fig. 7 shows the simulation model of hybrid system, implemented in MATLAB. Table I shows parameters of PV system and Table II shows parameters of DFIG and the wind turbine. Table III shows parameters of the applied controllers.

Preprints (www.preprints.org) | NOT PEER-REVIEWED | Posted: 26 November 2017 doi:10.20944/preprints201711.0169.v1

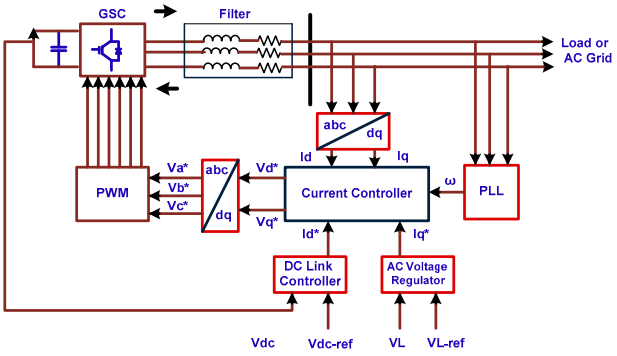

Fig. 5. Schematic diagram of grid side converter control.

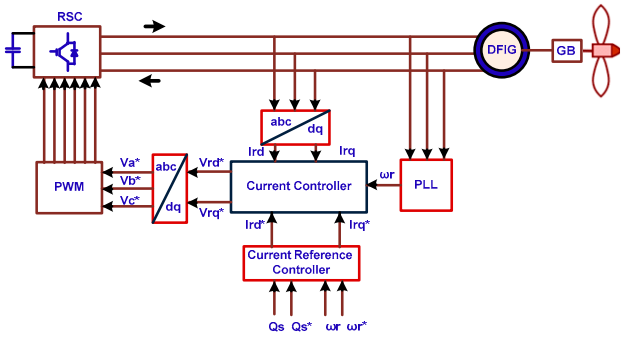

Fig. 6 Schematic diagram of rotor side converter control.

4. Simulation Results

Eight different cases are considered here with varying the weather conditions, load amount and load type. A ± 10 % of the wind speed and irradiance are examples of different weather conditions. A change in active or reactive power load demands is simulated. Finally, the system performance in the case of induction motor as a load is investigated.

Table 1 PARAMETER OF PV SYSTEM

Module name: Sun power SPR-305E-WHT-D		
open circuit voltage	(V)	64.2
Short circuit current	(A)	5.96
Maximum power	(W)	305.226
number of parallel modules		66
number of series modules		5
Shunt resistance	(Ω)	269.5934
Series resistance	(Ω)	0.37152
Total power of PV	(KW)	100

Preprints (www.preprints.org) | NOT PEER-REVIEWED | Posted: 26 November 2017 doi:10.20944/preprints201711.0169.v1

Table 2 PARAMTERES OF DFIG-WT

Rated power	kW	300
Rated stator voltage	(V)	400
Pair of poles		3
Stator and rotor resistance (R_s, R_r)	pu	0.023 - 0.016
Stator and rotor leakage inductance (L_{ls},L_{lr})	pu	0.18 - 0.16
Magnetizing inductance L_m	pu	2.9
rated DC-link voltage	(V)	800
rated wind speed	(m/s)	15

Table 3 PARAMTERES OF controller

DC link controller	K_{p1}	1.08
	K_{i1}	0.5
Ac voltage controller	K_{p2}	10
	K_{i2}	100
Current controller of grid side converter	K_{p3}	8.3
	K_{i3}	30
Current controller of rotor side converter	K_{p4}	0.1
	K_{i4}	0.005

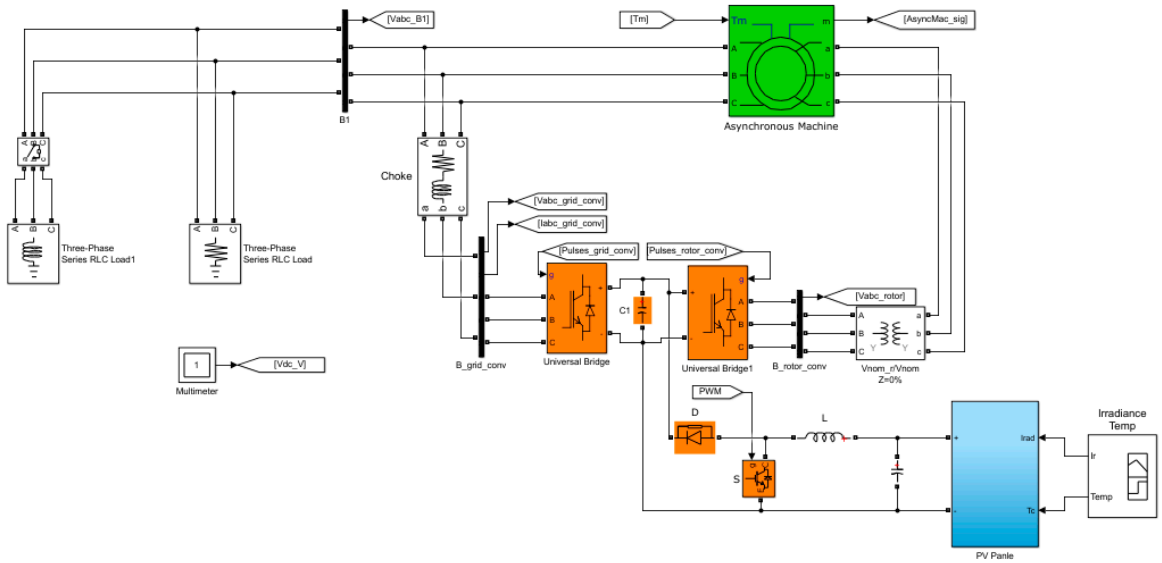

Fig. 7 Wind turbine with photovoltaic model.

Case 1:

In this case the irradiance to photovoltaic is 1000 W/m², and the wind speed to wind turbine is 15 m/s. Initially, the system load is purely resistive and an inductive load of 200 kVAr is applied as a step at time of 0.1 s

Preprints (www.preprints.org) | NOT PEER-REVIEWED | Posted: 26 November 2017 doi:10.20944/preprints201711.0169.v1

Table 4 PV, WT, AND LOAD PARAMETERS- Case 1

PV Power	WT Power	Resistive Load	Inductive Load
100 kW	200 kW	200 kW	100 kVAr

Fig. 8 displays the GSC current components. The d-component of the GSC current is not affected by the load step, as it is a step in reactive power but the q-component responded to the change and jumped to 0.45 pu, approximately in order to respond to the reactive power demand. The MPPT was able to keep the solar output unchanged as illustrated in Fig. 9a, but the wind active power has decreased slightly due to the slight decrease in the output voltage (Fig. 9c). The reactive power demand was fulfilled by the DFIG as depicted in Fig. 9b.

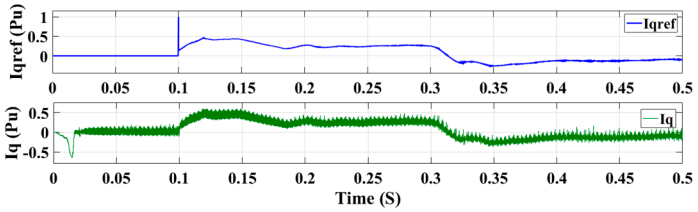

Fig. 8 Control signal of grid side converter, case 1.

The dc-link voltage is almost constant as illustrated in Fig. 9d as well as the PV voltage and current (Fig. 9e)

Case 2: 8 % increase in wind speed

In this case the irradiance to photovoltaic is 1000 W/m², and the wind speed to wind turbine is 15 m/s from 0 to 0.2 s and increased to 16.2 m/s (8%) from 0.2 to 1 s. The power ratings of the system are given in Table 5.

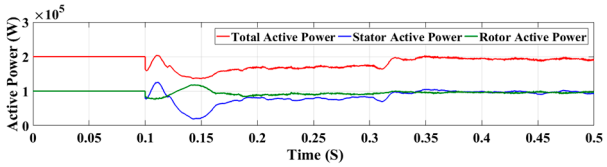

(a)

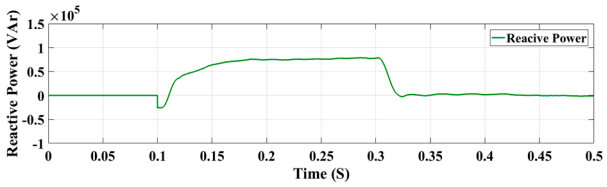

(b)

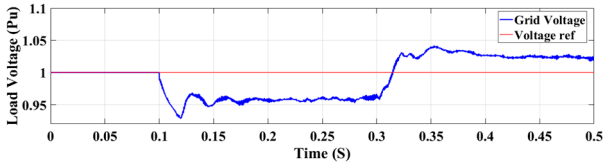

Preprints (www.preprints.org) | NOT PEER-REVIEWED | Posted: 26 November 2017 doi:10.20944/preprints201711.0169.v1

(c)

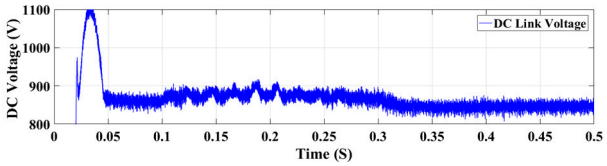

(d)

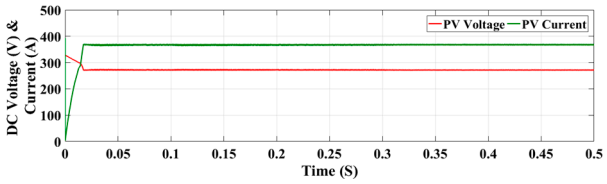

(e)

Fig. 9 (**a**) Active power, (**b**) reactive power, (**c**) Grid voltage (**d**), and (**e**)DC link voltage, PV voltage and current. Case 1

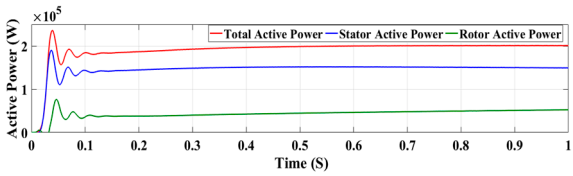

(a)

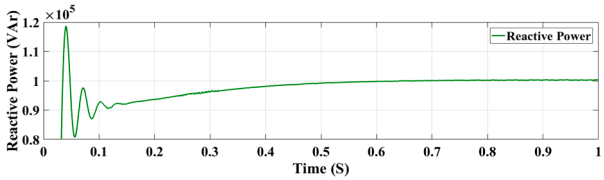

(b)

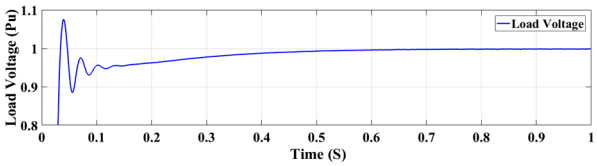

(c)

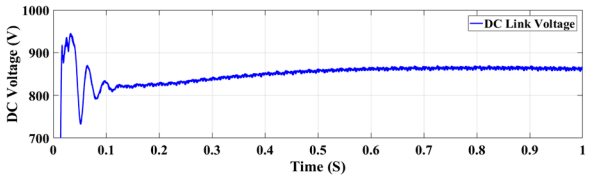

Preprints (www.preprints.org) | NOT PEER-REVIEWED | Posted: 26 November 2017 doi:10.20944/preprints201711.0169.v1

(d)

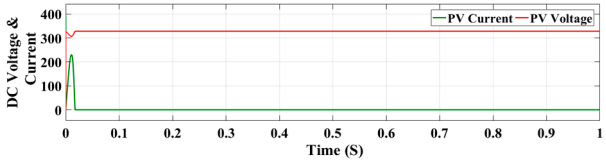

(e)

Fig. 10 (a) Active power, (b) reactive power, (c) Grid voltage (d), and **(e)** DC link voltage, PV voltage and current. - case 2

Table 5 PV, WT, AND LOAD PARAMETERS- Case 2

PV Power	WT Power	Resistive Load	Inductive Load
100 kW	250 kW	200 kW	100 kVAr

If the wind turbine is allowed to run at this speed, as done here, there will be a surplus in power of approximately 26 %. In order to accommodate this surplus, one of the solutions is reduce the PV output power. The power demand was met by the stator and the rotor of the DFIG as displayed in Fig. 10a and 10b. The load and dc-link voltages settled at their rated values as evident in Fig. 10c and 10d. In this case, the PV power was safely reduced to zero (Fig. 10e) and all the load power is supplied by the DFIG.

Case 3: 9.4 % decrease in the wind speed

In this case the irradiance to photovoltaic is 1000 W/m², and the wind speed to wind turbine is 15 m/s from 0 to 0.2 s and decreased to 13.6 m/s from 0.2 to 1 s. The generation and loading requirements are given in Table 6.

Now, there is a deficit in power of about 25% compared to the normal operating conditions. However, the total load demand can be met with the available powers of the hybrid system. Due the decrease in wind speed, the stator power has decreased as seen in Fig. 11a. The MPPT of the PV is able restore the load power and the load voltage as well as the dc voltage as illustrated in Fig. 11.

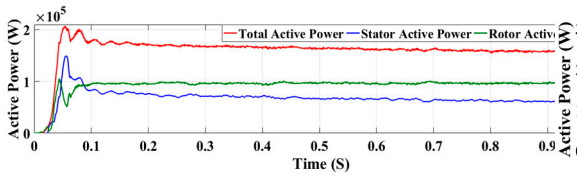

(a)

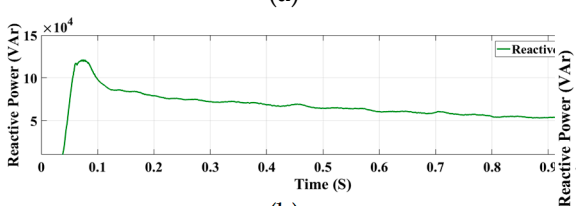

(b)

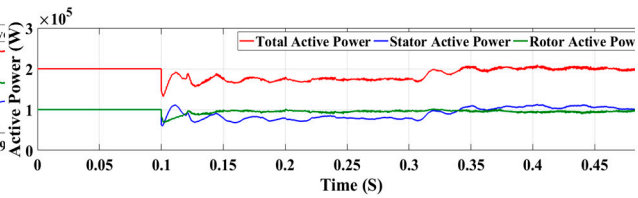

(a)

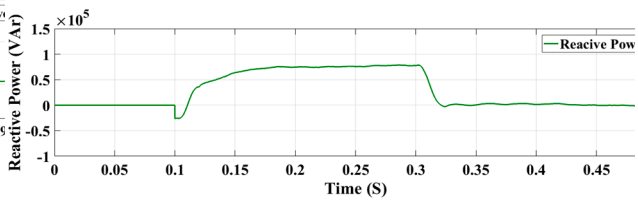

(b)

Preprints (www.preprints.org) | NOT PEER-REVIEWED | Posted: 26 November 2017 doi:10.20944/preprints201711.0169.v1

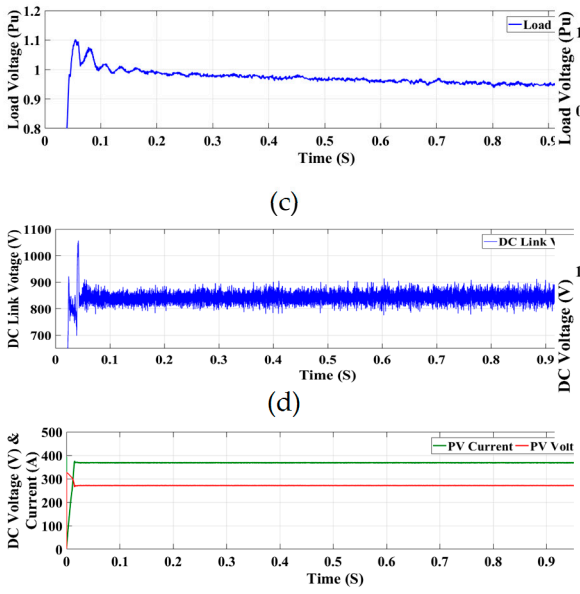

Fig. 11 (a) Active power, (b) reactive power, (c) Grid voltage (d), and DC link voltage, PV voltage and current- case 3.

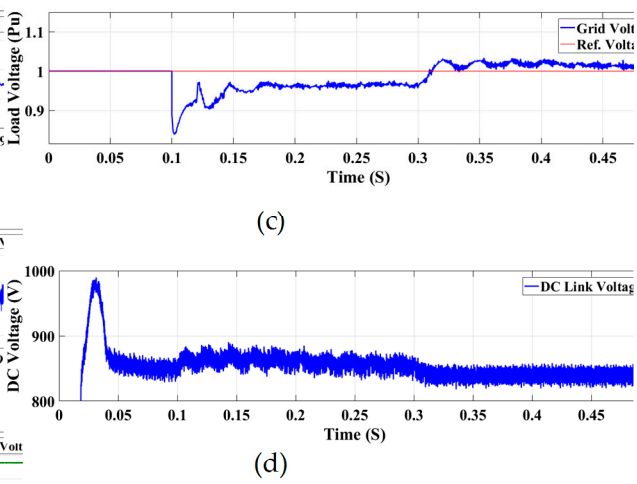

Fig. 12 (a) Active power, (b) reactive power, (c) Grid voltage (d), and DC link voltage, PV voltage and current. – Case 4

166

167 **Case 4: 20 % dectrease in the irridiance**

168 In this case the irradiance to photovoltaic is decreased to 800 W/m², and the wind speed is 15
169 m/s. There is also a step-in load reactive power at 0.1 s. The generation and loading requirements are
170 given in Table 7.

171 **Table 7** PV, WT, AND LOAD PARAMETERS – Case 4

PV Power	WT Power	Resistive Load	Inductive Load
80 kW	200 kW	200 kW	100 kVAr

172 The response is similar to case 1 where the load voltage has dipped slightly to 96 % and
173 consequently the load power also slightly dropped as seen in Fig. 12. Apart from the little voltage
174 dip, the system is able to provide the load power and the dc-link voltage is kept unchanged.

175 **Case 5: A 25 % increase in the resistive load**

176 In this case the irradiance to photovoltaic is 1000 W/m², and the wind speed to wind turbine is
177 15 m/s. the resistive load is increased 25 % compared the previous cases, as shown in Table 9.

178 **Table 8** PV, WT, AND LOAD PARAMETERS- case 5

PV Power	WT Power	Resistive Load	Inductive Load
100 kW	200 kW	250 kW	100 kVAr

179 The hybrid system responded satisfactorily to the load demand as shown in Fig. 13.

Preprints (www.preprints.org) | NOT PEER-REVIEWED | Posted: 26 November 2017 doi:10.20944/preprints201711.0169.v1

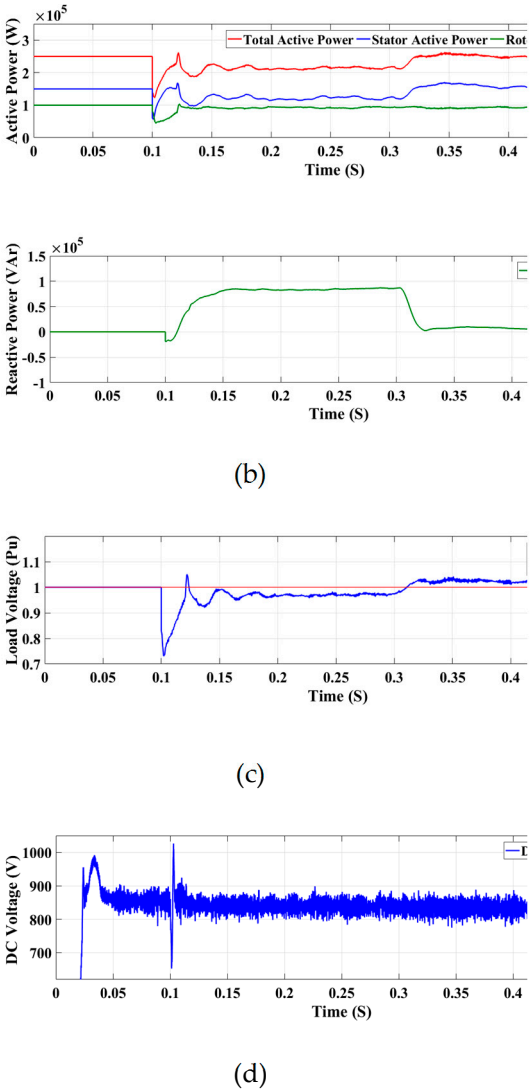

Fig. 13 (a) Active power, (b) reactive power, (c) Grid voltage (d), and DC link voltage, PV voltage and current.

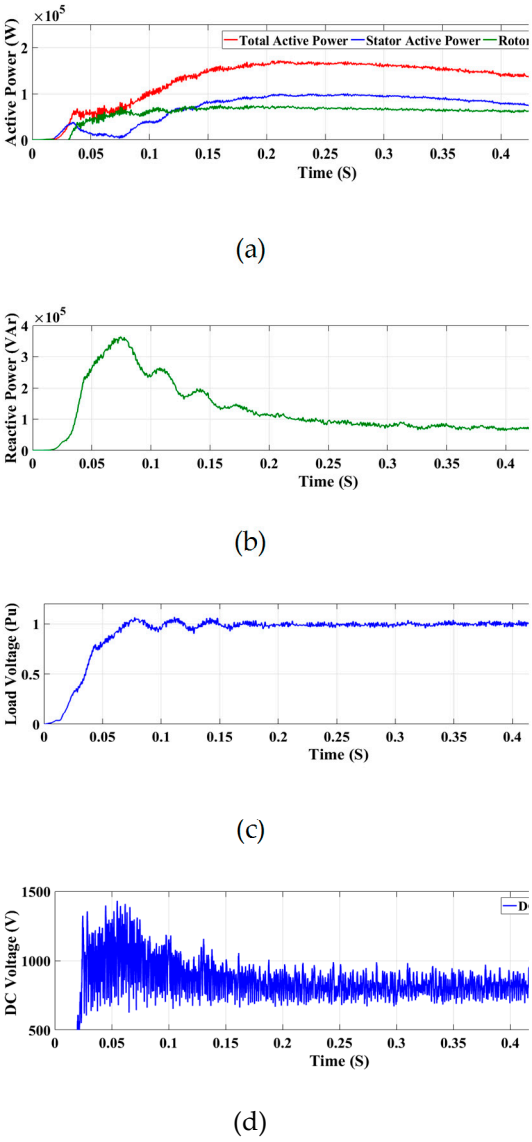

Fig. 14 (a) Active power, (b) reactive power; (c) Grid voltage (d), and DC link voltage, PV voltage and current.

Case: 6

In this case the irradiance to photovoltaic is 1000 W/m², and the wind speed to wind turbine is 15 m/s. variation load to induction motor with load details shown in Table 9.

Table X PV, WT, AND LOAD PARAMETERS-case 6

PV Power	WT Power	Induction motor	
100 kW	200 kW	180 kW	87 kVAr

The induction motor needed about 0.3 to reach its final speed as displayed in Fig 14. The system was able to cope with the dynamics of the induction motor and deliver the power demand. The load voltage stabilized at 1 pu and the dc-link voltage reached its reference value, 850 V.

5. CONCLUSION

An extensive study on the steady state performance of a hybrid PV-Wind system was presented in this paper. The wind system exploited a doubly-fed induction generator because it offers a high flexibility in control. In order to increase the system efficiency, the PV system was controlled by a maximum power point tracker. The operation of the hybrid system was investigated under various weather conditions such as changes in the wind speed and the irradiance. In the case of increased wind speed above 15 m/s, the system operator has many options such as decrease the PV output power or regulate the wind turbine around its nominal value. Various loading conditions were tested in this work also such as static and dynamic loads. The static loads included resistive and inductive loads while the dynamic loads were represented by an induction motor. The hybrid system responded satisfactorily in all cases.

REFERENCES

[1] M. S. ElSobki, "Egypt's renewable energy," Ministry of Electricity and Renewable Energy (MoE&RE), April, 14th, 2016.
[2] KH. Hussein, I. Muta, T. Hoshino, and M. Osakada "Maximum photovoltaic power tracking an algorithm for rapidly changing atmospheric condition," IEEE Proc. Generation Transmission Distribution, pp. 59–64, vol. 142, no. 1, Jan 1995.
[3]L.K. Lettinga, J. L. Mundaa, and Y. Hamam, "Dynamic performance analysis of an integrated wind-photovoltaic microgrid with storage," International Journal of Smart Grid and Clean Energy, pp. 307-317, vol. 3, no. 3, July 2014.
[4] M.S. Fathy, A. H. K. Alaboudy, and Th.ELShater," Night operation of a photovoltaic system,"proc. of the 15th international Middle East power system conference (MEPCON'12), December 23-25, 2012, paper ID 189. Alex. Egypt.
[5] D. Nguyen, and G. Fujita, "Dynamic response evaluation of sensorless MPPT method for hybrid PV-DFIG wind turbine system," Journal of International Council on Electrical Engineering, pp. 49–56,vol. 6, no. 1, 08 November 2016.
[6] Rajesh K., A.D Kulkarnib, and T.Ananthapadmanabhab, "Modeling and simulation of solar PV and DFIG based wind hybrid system," Procedia Technology, pp. 667 – 675, August 2015,
[7] M. Nayeripour, and M. Hoseintabar, "A comprehesnive dynamic modeling of grid connected hybrid renewable power generation and storage system," International Journal of Modeling and Optimization, pp.62-65, Vol. 1, No. 1, April 2011.
[8] B. Hamdan,and N.Anwer, "An integrated hybrid power system based on solar PV array and wind turbine doubly fed induction generator for basrah, Iraq," International Journal of Science & Technology, pp.,11-20, vol. 2, no, 3, June, 2012.
[9] M. Zanganeh, and F. Norouzi, "Evaluating load current and MPPT algorithms for the solar energy with an emphasis on DC systems," Research Journal of Recent Sciences, pp.1-5, vol. 4, 1-5, March (2015).
[10] Mrs. S. Sathana and Ms. Bindukala M.P., "Hybrid solar and wind power conversion using DFIG with grid power levelling," International Journal of Emerging Trends in Electrical and Electronics (IJETEE),pp.43-48, vol. 1, no. 1, March,2013.
[11] Aparna K P, Priya R, and S.Suryanarayanan, "Modeling and simulation of a PV system using DC-DC converter," International Journal of Latest Research in Engineering and Technology (IJLRET), PP.09-16, vol. 1, no. 2, July, 2015.
[12] R. Pena, J.C.Clare,and G. M. As her, "Doubly fed induction generator using back-to-back PWM converters and its application to variables peed wind-energy generation," IEE Puoc.-Electr. Power Appl.,pp. 231-241, vol. 143, no 3, May 1996.
[13] A. A. Tanvir, A. Merabet, and R. Beguenane," Real-time control of active and reactive power for doubly fed induction generator (DFIG)-based wind energy conversion system," Energies ISSN 1996-1073,pp.10389-10408, September 2015.